Chinese Chemical Letters 35 (2024) 109378

Contents lists available at ScienceDirect

Chinese Chemical Letters

journal homepage: www.elsevier.com/locate/cclet

Progress of additives for morphology control in organic photovoltaics

Zhongjie Li[1], Xiangyue Kong[1], Yuhao Liu, Huayu Qiu*, Lingling Zhan*, Shouchun Yin*

Key Laboratory of Organosilicon Chemistry and Materials Technology of Ministry of Education, College of Material, Chemistry and Chemical Engineering, Hangzhou Normal University, Hangzhou 311121, China

ARTICLE INFO

Article history:
Received 24 October 2023
Revised 5 December 2023
Accepted 5 December 2023
Available online 11 December 2023

Keywords:
Organic photovoltaics
Additives
Active layer morphology
Mechanisms
Photovoltaic performances

ABSTRACT

The microstructure of the active layer in organic photovoltaics (OPVs), such as the size of phase separation, purity of the phases, and molecular packing within each phase, plays a crucial role in influencing the behavior of excitons and charge carriers within the active layer. It is also a key determinant of the photovoltaic performance of the device. During the optimization of OPV devices, the use of additives has been demonstrated to be an effective strategy in microstructure control, leading to enhanced performance. Therefore, the quest for stable and efficient novel additives, along with an exploration and summarization of the mechanisms underlying additive-induced microstructure control, is essential for a better understanding of the developmental trends of high-performance additives. In this review, we categorize additives based on their chemical structures and discuss their effects on the microstructure of the active layer from both thermodynamic and kinetic perspectives. Furthermore, we elaborate on the working mechanisms and their impact on the photovoltaic performance of the devices. This review provides an overview of recent advances in additives for OPVs, offering potential guidance for the future development of additives and further optimization of the active layer in photovoltaic devices.

1. Introduction

Organic photovoltaics (OPVs), characterized by their light weight, flexibility, low cost, and solution-processability, are considered as a promising renewable energy technology [1–9]. At present, high-efficiency OPVs typically incorporate a bulk heterojunction (BHJ) as the photovoltaic active layer [10]. The BHJ structure consists of a blend of electron donor (D) and electron acceptor (A) materials [11–13], forming an interpenetrating network of donor-acceptor domains [14,15].

In the active layer of OPVs, solar energy undergoes five key processes for conversion to electricity (Fig. 1). (1) Exciton generation: Sunlight prompts electrons to transition, forming excitons—an electron-hole pair due to Coulombic interactions [16]. (2) Exciton diffusion: Confined excitons move within donor or acceptor phases. (3) Exciton dissociation (charge generation): At the D-A interface, energy offset drives dissociation, yielding mobile charge carriers. (4) Charge transport: Free carriers migrate within pure phases, with electrons in the acceptor and holes in the donor [17]. (5) Charge collection: Carriers are gathered at respective electrodes, creating an electric field and voltage. When the device connects to an external circuit, the device generates photocurrent [18–20], and the behavior of excitons and carriers depends on the microstructure of the active layer, which is crucial for OPV performance.

How does the microstructure of the active layer affect photovoltaic performance? In the BHJ active layer, due to a certain degree of compatibility between donor and acceptor materials [21], three phases are generally recognized: relatively pure donor and acceptor phases [22], as well as a mixed donor-acceptor phase. The mixed donor-acceptor phase enables exciton dissociation, resulting in charge carriers moving to electrodes through their respective phases. Incompatibility between donor and acceptor materials or excessive self-aggregation leads to over-separation [23,24], limiting the diffusion distance of excitons and causing monomolecular recombination [25]. While good miscibility enhances donor-acceptor interfaces for dissociation, it may also increase severe bimolecular recombination. Inadequate connectivity traps carriers [26] hinder their migration to electrodes. Therefore, improving phase purity could reduce internal defects, and lowering the chance of recombination. The packing and intensity of active molecules significantly affect photovoltaic performances [27–29]. However, without proper post-treatment, BHJ films prepared from a single solvent may lack the optimal microstructure, resulting in subpar photovoltaic performance. Optimizing the morphology of active layer films is pivotal for advancing OPV devices. Various post-treatment

* Corresponding authors.
E-mail addresses: huayuqiu@163.com (H. Qiu), linglingzhan@hznu.edu.cn (L. Zhan), yinsc@hznu.edu.cn (S. Yin).
[1] These authors contributed equally to this work.

https://doi.org/10.1016/j.cclet.2023.109378
1001-8417/

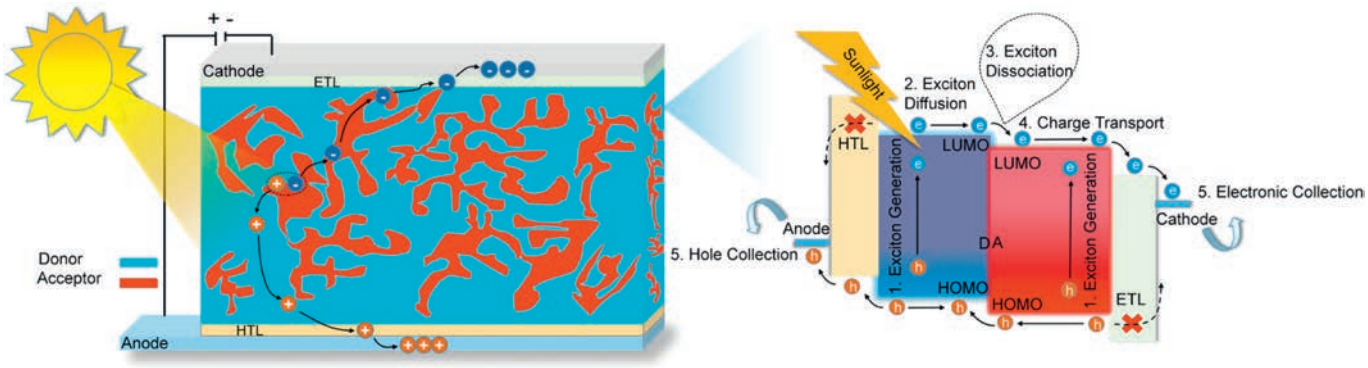

Fig. 1. Operation mechanism diagram of conventional OPVs.

techniques, including thermal spin-coating (TSC) [30], thermal annealing (TA) [31–33], solvent vapor annealing (SVA) [34–36], and additive tuning [37–47], have been proven to be effective. TSC involves controlled temperature film formation for optimal molecular stacking and orientation, though it may lead to lower reproducibility for quality device due to high requirement for the cooling rates. TA and SVA can also optimize morphology but may lead to limited voltage and extreme stacking, impacting molecular orientation and phase separation. Additive tuning (by adding a specific additive to active layer) stands out as a convenient and efficient method, in the advanced and highly efficiency OPVs, the optimal morphology and the desired photovoltaic performance were always obtained *via* additive combination with other post-treatment processes [48].

As the industrialization of OPVs approaches, there is an urgent need for the development and exploration of various types of additives and their working principles. This paper provides a comprehensive review of the classification and mechanisms of action of additives, starting from the fundamental approaches of morphology optimization: thermodynamics and kinetics [49]. The structure of the additives discussed in this review is shown in Fig. 2. Thermodynamic methods involve controlling intra- and intermolecular interactions of donor and acceptor molecules, and utilizing differences in solubility to control phase separation size and final active layer morphology. Kinetic methods involve various controls by additives over solution aggregation, film formation, and post-treatment, allowing for adjustments in crystallization and phase separation to control the final membrane morphology. Furthermore, additives will be categorized base on their functionality, including non-aromatic liquid additives and aromatic liquid additives for thermodynamic optimization, modified small molecule non-volatile solid additives, polymer non-volatile solid additives, phenyl-derived volatile solid additives, and some other types of additives for kinetic optimization. This review will provide a comprehensive overview of recent research progress on additive-induced control of active layer morphology in the past five years, showcasing current achievements in optimizing OPV active layer nanomorphology, with the aim of offering potential guidance for future optimization efforts in this field.

2. Liquid additives

Liquid additives typically exhibit high boiling points [50], characterized by their slow evaporation, which can significantly influence the nanostructure of the active layer [51]. Additionally, due to distinct interactions between the liquid molecules and the donor or acceptor components, they possess a certain dissolution selectivity that can modulate the compatibility between donor and acceptor (adjustment of intra- and intermolecular interactions) [52,53]. This enables liquid additives to thermodynamically optimize the morphology of the active layer. Consequently, this leads to alterations in the aggregation and phase separation of the donor-acceptor blend, ultimately influencing the crystallinity of the active layer and the device performances. This section categorizes liquid additives into non-aromatic and aromatic types to delineate their respective progress in morphology manipulation.

2.1. Non-aromatic liquid additives

During the film formation process of the active layer, some system exhibits suboptimal crystalline behavior [54]. Non-aromatic liquid additives possess high boiling points, allowing for a gradual evaporation process that facilitates the full induction of molecular arrangement. The selective solubility can be adjusted to promote a moderate phase separation between donor and acceptor materials, thereby encouraging a more ordered molecular stacking within the active layer.

In 2006, Bazan *et al.* introduced 1-octanethiol as a liquid additive into the organic active layer [55]. An excess of 1-octanethiol, combined with gold nanoparticles for plasmonic resonance enhancement, induced ordered P3HT crystallization, enhancing charge mobility in the BHJ film and resulting in higher photocurrent. Subsequently, Bazan and his colleagues discovered that 1,8-octanedithiol (ODT) as a liquid additive increased PCPDTBT:PC_{70}BM phase separation, and augmented the blend film root mean square roughness (RMS) and carrier lifetime, thereby enhancing device efficiency [56]. In 2018, Müller-Buschbaum *et al.* used ODT as a post-treatment additive for P3HT:PC_{71}BM to probe its mechanism [57]. AFM images (Fig. 3a) showed a film with 3 vol% ODT had a larger roughness (RMS = 8 nm) compared to the ODT-free film (RMS = 1 nm). This was attributed to ODT inducing greater phase separation between P3HT and PC_{71}BM due to their differing solubilities. During the film formation, PC_{71}BM diffused along the ODT evaporation path, leading to a larger donor-acceptor phase separation. This resulted in a dominant PC_{71}BM accumulation layer on the film surface (Fig. 3b), acting as an electron transport layer and greatly enhancing short-circuit current density (J_{SC}). Thus, ODT treatment effectively increased P3HT crystallinity, optimized internal morphology, and improved molecular compatibility, ultimately enhancing photovoltaic performance.

In 2008, Heeger *et al.* explored the impact of adding 1,8-diiodooctane (DIO) to the PCPDTBT:PC_{71}BM system [58]. At a 2.5 vol% concentration, DIO promoted phase separation between the polymer and fullerene, leading to improved photovoltaic performance. This addition resulted in purer-phase regions within the PCPDTBT polymer networks, facilitating hole transport. Utilizing DIO as a liquid additive increased the system's photoconversion efficiency from 3.4% to 5.1%. In 2018, Chen *et al.* utilized DIO as an additive for optimizing the PBTIBDT:PC_{71}BM system [52].

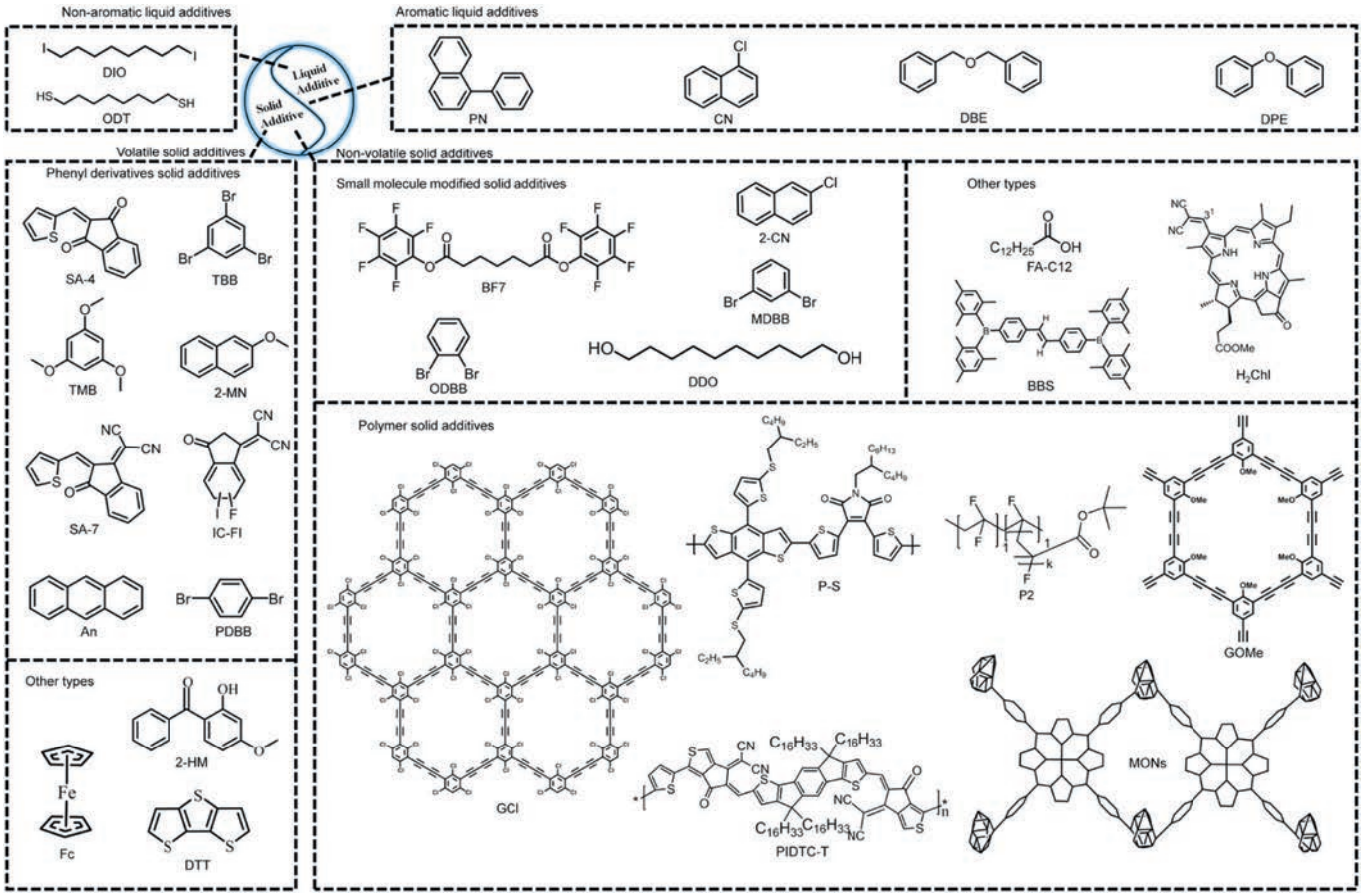

Fig. 2. Chemical structures of the liquid and solid additives discussed in this review.

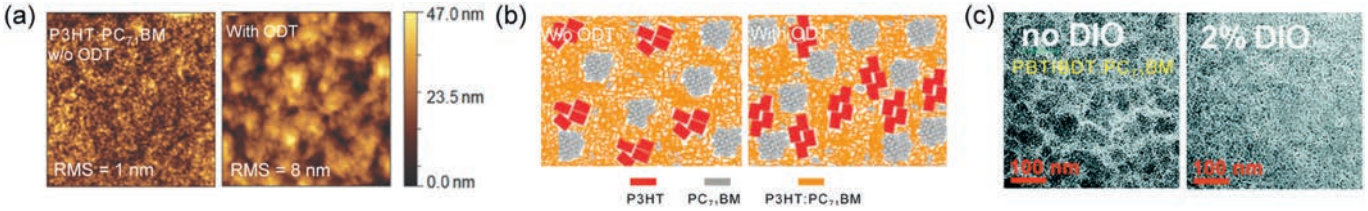

Fig. 3. (a) AFM height images of the P3HT:$PC_{71}BM$ blend film with and without ODT additive. Reproduced with permission [57]. Copyright 2018, John Wiley and Sons. (b) Scheme diagram of molecular arrangement of the P3HT:$PC_{71}BM$ blend film with and without DOT additive. (c) TEM images of the PBTIBDT:$PC_{71}BM$ blend film with and without DIO additive. Reproduced with permission [52]. Copyright 2013, The Royal Society of Chemistry.

TEM images (Fig. 3c) revealed that in the blend film without DIO, the donor polymer formed large dark domains within a lighter matrix, indicating higher concentrations of $PC_{71}BM$. Due to strong aggregation tendencies of the materials, this system exhibited a larger phase separation. With the addition of 2 vol% DIO, a crystalline morphology emerged within the BHJ, with $PC_{71}BM$ evenly dispersed throughout the film. Further investigation showed that DIO selectively dissolved $PC_{71}BM$ and aggregated the PBTIBDT polymer, reducing the size of $PC_{71}BM$ clusters and polymer donors. This led to an appropriate crystalline behavior, resulting in significant enhancements in photovoltaic performance. Finally, the system's efficiency increased from 2.32% to 5.36% At the same time, DIO also has a good morphology control effect on non-fullerene OPV [59]. In 2018 Chen *et al.* add DIO to 3-otcyl-2-(1,1-dicyanomethylene)rhodamine (A2):PTB7-Th non-fullerene small molecule system to explore its working mechanism [60]. It was observed that the addition of 1 vol% DIO made the blend film morphology of the A2:PTB7-Th system show ideal phase separation and uniform morphology. The smooth surface morphology is beneficial to minimizing the electrical leakage. Due to the improvement of FF and J_{SC}, a good PCE of 9.07% was finally obtained in the system.

2.2. Aromatic liquid additives

For non-fullerene acceptor systems, due to the striking similarity in molecular structures between donor and acceptor materials, they generally exhibit good compatibility [61]. Consequently, the phase separation size between the donor and the acceptor tends to be too small, to hinders efficient charge transport and collection. Aromatic liquid additives, by modulating intermolecular interaction, serve to adjust the miscibility between donor and acceptor materials in the active layer. This optimization leads to the refinement of the active layer film morphology.

In 2010, Bazan *et al.* developed naphthalene (CN) as a liquid additive to optimize the active layer morphology of [(4,4-didodecyldithieno[3,2-*b*:2′,3′-*d*]silole)-2,6-diyl-*alt*-(2,1,3-benzoxadiazole)-4,7-diyl] (P1):$PC_{71}BM$ system [62]. CN facilitated

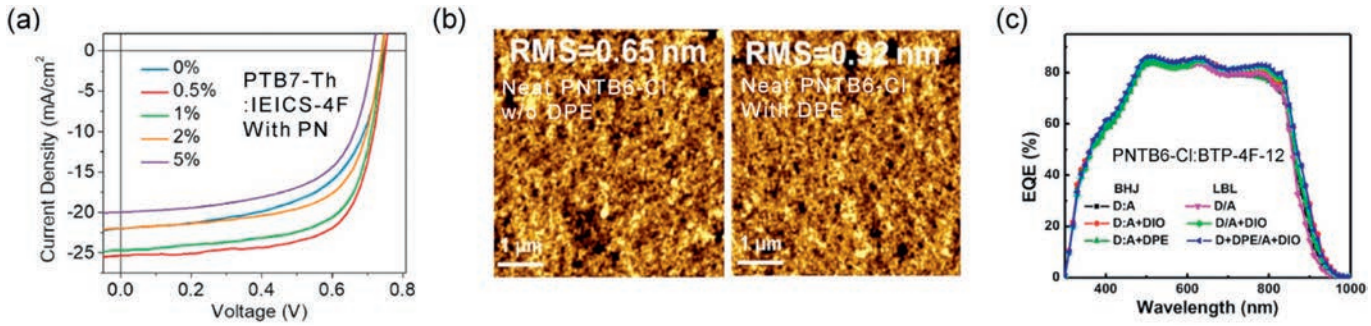

Fig. 4. (a) *J-V* characteristics of the BHJ and LBL type film with different contents of PN under the illumination of AM 1.5 G, 100 mW/cm^2. Reproduced with permission [64]. Copyright 2020, Elsevier. (b) AFM height and TME images of the neat PNTB6-Cl film with or without DPE additive. (c) EQE spectra of BHJ and LbL type OPVs based on PNTB6-Cl:BTP-4F-12 system. Reproduced with permission [51]. Copyright 2022, Elsevier.

P1 aggregation, enhancing the donor-acceptor phase separation and improving the active layer film morphology. In 2018, Wang *et al.* further enhanced the FTAZ:IDCIC system by adding CN as a liquid additive [63]. Achieving an appropriate phase separation and optimizing the donor-acceptor interface, while ensuring efficient exciton dissociation, reduced charge bimolecular recombination, resulting in the increased photocurrent and efficiency (from 9.64% to 13.58%). The study noted that IDCIC exhibited good solubility in CN, preventing excessive mixing within the donor during film formation, enhancing phase purity, larger phase separation, and improved crystallinity for both donor and acceptor.

While non-fullerene acceptors share some molecular similarities with polymer donors, allowing for high compatibility between them, it is essential to address the significant crystalline differences between small molecule acceptors and polymer donors in non-fullerene systems. In 2020, Ade *et al.* introduced 1-phenylnaphthalene (PN) as a liquid additive into the PTB7-Th:IEICS-4F system [64]. The AFM image of the active layer morphology, showed an increase in domain size in the blend film with 0.5 vol% PN additive compared to the film without additives. The study revealed that PN additive played a crucial role in enhancing the ordered molecular stacking of IEICS-4F, augmenting the secondary crystal order and promoting good phase purity within the active layer film. This morphology proved more conducive to charge transport, resulting in higher J_{SC}, as shown in Fig. 4a, 0.5 vol% PN can maximize the photovoltaic performance, and the efficiency of this system increased from 9.7% to 13.3%. In 2022, Zhang *et al.* employed diphenyl ether (DPE) as a liquid additive using a layer-by-layer (LbL) deposition process to incorporate it into the donor layer of the PNTB6-Cl:BTP-4F-12 system [51,65]. The AFM images depicted changes in the donor layer morphology, as depicted in Fig. 4b, revealed that the RMS value of the pure film after additive treatment (0.92 nm) was higher than that of the original film (0.65 nm). Additionally, TEM images of the DPE-treated donor pure film displayed a denser, granular structure. The study indicated that DPE acted on the donor, leading to the formation of a more swellable matrix for exciton diffusion. This was conducive to hole transport within the donor layer. As shown in Fig. 4c, the external quantum efficiency (EQE) spectral edge of LbL-type OPV treated with DPE additive can be significantly extended in the long wavelength region.

Research has shown that all-polymer OPVs possess distinct advantages in operational stability and processability [66–68]. However, in all-polymer systems, where both the donor and acceptor materials are polymers, controlling the morphology of the active layer is more challenging compared to systems involving small molecules. This often leads to limitations in charge mobility and severe charge recombination, resulting in subpar photovoltaic performance of the devices. In 2019, Huang *et al.* introduced dibenzyl ether (DBE) as a liquid additive to induce ordered nanostructures in the active layer (PBTA-Si:PTzBI-Si:N2200 system) [69], inherently suppressing charge recombination losses. The AFM study of the morphological changes in the active layer induced by DBE, demonstrated larger domain sizes in the blend film treated with DBE. The study noted that the high-boiling-point DBE provided more time for polymer chain rearrangement, leading to a denser and longer polymer fiber morphology in the film, thereby enhancing exciton migration rates and the final photovoltaic efficiency.

3. Solid additives

The slow evaporation and residual effects of high-boiling-point liquid additives may lead to photo oxidation of the active layer, ultimately reducing the operational stability of OPV devices [48]. In contrast to the optimizing role of liquid additives on the active layer, which involves adjusting the solubility of active materials in solvents and their intra/intermolecular interactions, solid additives operate through dynamically optimizing interactions between additive molecules and donor-acceptor molecules during the active layer formation process, as well as crystallinity and molecular orientation during post-treatment after film formation [46]. As a result, the pursuit of solid additives that confer excellent stability to the active layer has emerged as a focal point in OPV additive research. Based on the physical properties of solid additives, they can be categorized as volatile solid additives and non-volatile solid additives.

3.1. Non-volatile solid additives

Non-volatile solid additives, owing to their distinctive molecular structures or functional groups, engage in intermolecular interactions with target molecules [70]. This interaction enables them to modulate molecular arrangement and stacking, ultimately influencing the nanostructure of the active layer. In this section, we will discuss the impact of non-volatile solid additives on the formation morphology of the active layer from a kinetic perspective, both before and after the film-forming process.

3.1.1. Small molecule modified solid additives

As mentioned before, both DIO and ODT have been established as effective liquid additives. In 2021, Chen *et al.* introduced a solid additive 1,10-decanediol (DDO) and incorporated it into the PM6:Y6 system for optimization [71]. DDO was introduced into the donor layer using a sequential deposition method, while CN was added to the acceptor layer. The characteristics of the active layer morphology were observed, AFM results revealed that DDO acted on the polymer donor, enhancing the film density and crystallinity of PM6. The study pointed out that with the addition of DDO, the

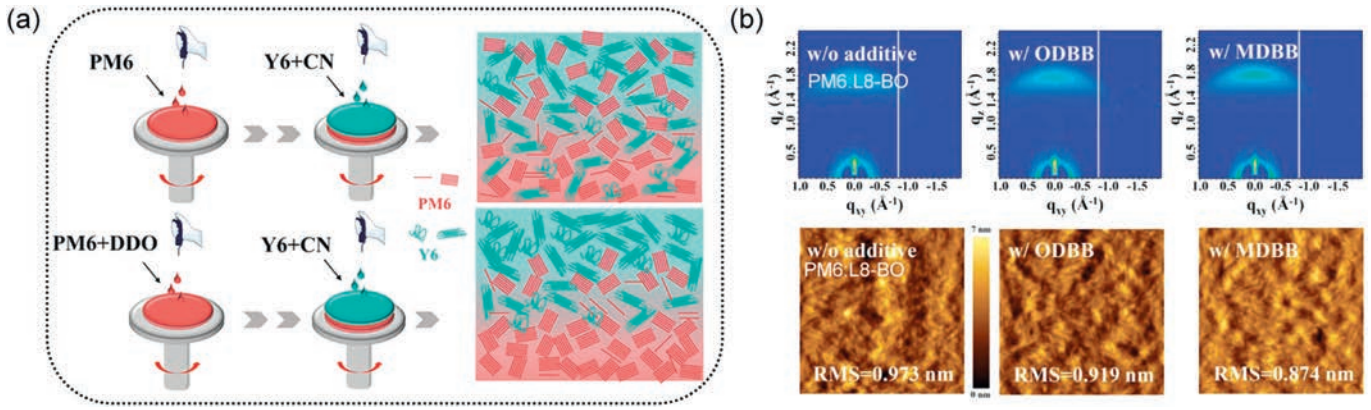

Fig. 5. (a) Scheme diagram of molecular arrangement of the PM6:Y6 LBL type film with or without DDO additive. Reproduced with permission [71]. Copyright 2021, John Wiley and Sons. (b) GIWAXS patterns and AFM height images of the PM6:L8-BO blend film with or without ODBB, MDBB, additive. Reproduced with permission [44]. Copyright 2023, John Wiley and Sons.

PM6 layer was only partially infiltrated by the Y6 solution. Consequently, DDO doping effectively prevented excessive mixing of PM6 and Y6 in the LbL process after film formation. This resulted in an ideal vertical phase separation with enriched PM6 at the anode and Y6 at the cathode, as shown in Fig. 5a, ultimately yielding commendable fill factor (FF). With the optimization provided by DDO, the system's efficiency increased from 15.67% to 16.93%.

Halogens, due to their ability to induce strong intermolecular interactions, have become commonly be used modifying substituents in molecular design. In 2022, Cheng *et al.* incorporated the multi-fluorinated molecule BF7 into the PM6:Y6 system to explore its impact on solid additive morphology regulation [72]. BF7′s action was linked to PM6 and Y6 phase separation and the two-stage crystallization process. The timing of Y6′s separation from PM6′s weakly ordered network during active layer formation was influenced by the F-π non-covalent interaction between BF7′s perfluorinated benzene and Y6′s difluorinated benzene FIC end group. This led to more ordered and oriented crystal nanodomains. Consequently, the system's efficiency rose from 15.09% to 16.86%. Notably, a similar effect was observed in the PM6:IT-4F system, affirming BF7′s favorable optimization on difluorinated benzene end groups of acceptors.

Halo-substituted additives effectively enhance the photovoltaic performance of devices, and isomeric halogen molecules also have distinct effects on optimizing the active layer. In 2023, building upon the success of the classic liquid additive CN, Yan *et al.* employed its positional isomer, 2-CN, as a solid additive to optimize the D18-Fu:L8-BO system [70]. The study elucidated those interactions between 2-CN and L8-BO prior to active layer formation induced an enhanced dipole moment perpendicular to the acceptor molecule plane, prompting the aggregation of acceptor molecules in the blend film, allowing for faster nucleation and crystallization of the acceptor. This, in turn, elevated exciton mobility, resulting in an efficiency boost from 17.4% to 18.4%. In 2023, Hou *et al.* introduced positional isomers ODBB, MDBB, featuring dibromo-benzene moieties, into the PM6:L8-BO system to observe the impact of these isomeric additive molecules on the optimization of the active layer morphology [44]. Notably, ODBB significantly enhanced the system's efficiency from 16.28% to 18.42%. The GIWAXs images of the active layer, as illustrated in Fig. 5b, revealed stronger π-π interactions and shorter stacking distances in the blend films treated with the additives. The robust non-covalent interactions between the additives and L8-BO led to a reduction in the π-π stacking distance between L8-BO molecules. AFM results demonstrated a more pronounced fibrous network structure on the film surface when all three isomeric additives participated in the film formation process. The optimized active film with ODBB exhibited well-organized domain structures, facilitating efficient exciton dissociation and ultrafast charge transfer.

3.1.2. Polymer solid additive

The all-polymer system exhibits excellent long-term operational stability [73]. However, the limited charge carrier mobility within the active layer has constrained the development of all-polymer devices. The introduction of polymer additives into small molecule-based system has emerged as a hotspot in recent years for morphology optimization in OPVs [74].

In 2020, Yang *et al.* introduced the organic ferroelectric polymer PVDF-*g*-PBA (P2) as a solid additive in the PM6:IT-4F system to modify its morphology [75]. TEM images (Fig. 6a) showed that the blend film with P2 had a smooth and uniform morphology, contrasting with the initial film rich in $PC_{71}BM$. GIXD images revealed no impact on molecular stacking and orientation. Further studies found that NMP solvent facilitated ferroelectric polarization, creating an intrinsic electric field that enhanced charge transfer efficiency, and resulting in increased photocurrent. Ultimately, P2 improved the system's efficiency from 10.6% to 11.83%. In 2020, Li *et al.* employed the chlorinated graphyne (GCl) conjugated polymer as a solid additive to optimize the PM6:Y6 system [76]. The study elucidated that GCl could alter the crystallization habits of materials during the film formation process. In the active layer formation process, GCl acted as a nucleation center to induce the crystallization of either the conjugated polymer or non-fullerene acceptor. This crystallization behavior could be classified as heterogeneous nucleation, which was conducive to exciton dissociation and charge transport, resulting in increased J_{SC} and FF for the system.

In 2022, Gao *et al.* utilized methoxy–substituted graphene (GOMe) as a solid additive to optimize the ZnP-TSEH:6TIC system, enhancing the system's efficiency from 15.15% to 17.18% [77]. The addition of GOMe to the acceptor layer increased its aggregation, significantly promoted acceptor diffusion and resulted in a favorable vertical composition distribution, tightly packed molecular stacking for morphology optimization of the active layer. In the same year, Foster *et al.* introduced another organic metallopolymer (MONs) as a solid additive into the PffBT4T2OD:PCBM system [78]. The GIWAXS images revealed a well-defined in-plane π-π stacking in the active layer blend film containing MONs, indicating strong molecular ordering. AFM images (Fig. 6b) illustrated that the addition of MONs led to reduce nano-structural domain size and increase phase separation in the active layer film, enhancing crystallinity. The study noted that due to the parallel alignment of MONs on the surface, they acted as templates during the spin-

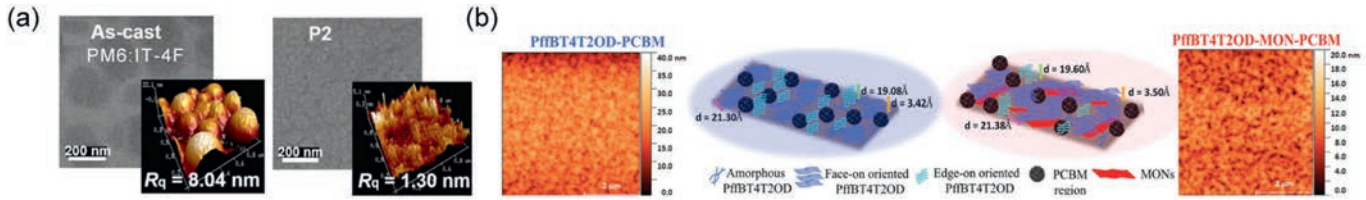

Fig. 6. (a) AFM height and TME images of the PM6:IT-4F blend film with or without P2 additive. Reproduced with permission [75]. Copyright 2020, Elsevier. (b) AFM height images and scheme diagram of molecular arrangement of the PffBT4T2OD:PCBM blend film with or without MON additive. Reproduced with permission [78]. Copyright 2022, John Wiley and Sons.

coating process, and elevated the crystallinity and orientation of surrounding active molecules, consequently improving charge mobility and achieving higher J_{SC}. This enhancement resulted in an efficiency boost of the system from 10.6% to 12.3%. These two reports provide valuable guidance for the application of organic metallopolymer as solid additives.

The multi-component strategy has been demonstrated as an effective approach for morphology control [65,79-81]. By designing molecular frameworks with similar characteristics and regulating intermolecular interactions, morphology optimization can be achieved. Building on this concept, researchers propose the application of this strategy in designing and developing novel solid additives. In 2020, Yan *et al.*'s study provided valuable insights into utilizing polymers as additives for active layer photovoltaic materials [82]. They employed a thiophene-fused end-capped polymer (PIDTC-T) as a solid additive to optimize the PM6:Y6 system. PIDTC-T improved system compatibility, thereby reducing the initial oversized phase separation in the film. This augmentation led to enhance exciton diffusion and charge transfer efficiency, resulting in a remarkable efficiency improvement, elevating the system's performance.

In addition to drawing inspiration from small molecule acceptor frameworks for designing solid additives, high-performance polymer donor molecules also serve as excellent building blocks for solid additive design units. In 2023, Peng *et al.* introduced a polymer solid additive (P-Cl) with electron-donating properties into the PM6:BTP-eC9 system for optimizing the active layer morphology [83], significantly boosting the system's efficiency from 17.36% to 19.10%. The combination of LbL with the polymer additive preserved PM6′s weak self-assembly, facilitating BTP-eC9 penetration and forming an intertwined donor/acceptor dual-continuous network. This structure enabled efficient charge transport and extraction.

3.1.3. Other types of non-volatile solid additives

Effective exciton diffusion and charge transport play a vital role in improving the performances of OPVs. Organoboron as a functional solid additive, has been proved to be positive for exciton diffusion and charge transport. In 2022, Zhan *et al.* added organoboron BBS to PM6:Y6 system and found that BBS could optimize the stacking of Y6 molecules, resulting an excellent PCE of 17.6% [84]. As presented in the GIWAXs results (Fig. 7a), compared to the control active layer, BBS helps to improve the π-π stacking of Y6 molecules. With the additive of BBS, the aggregation model of the active molecular convert from a lower *H*-type aggregate to a higher *J*-type aggregate, increasing exciton diffusion, and enhancing the order of the main chain caused by the π-π stacking of the terminal groups, which contributes to intermolecular electron transport. This study greatly improves the performance of PM6:Y6 system by applying a simple morphology optimization strategy.

In the pursuit of eco-friendly OPVs, it is crucial to consider not only performance but also aspects like toxicity, environmental impact, and biocompatibility in usage and recycling [85–87]. In 2023, Chen *et al.* incorporated fatty acid-based solid additives (FA-C12) into the PM6:Y6 system [88], observing their morphological impact (Fig. 7b). The RMS of pristine PM6 film decreased slightly from 1.23 nm to 1.19 nm with 10 wt% FA-C12. FA-C12, acting as an impurity, hindered PM6 fiber stacking, enhancing film swelling. Its favorable compatibility with chloroform solvent facilitated Y6 diffusion into PM6 during film formation, promoting mutual donor-acceptor diffusion. This induced a more favorable vertical phase separation, resulting in higher exciton dissociation, charge transport, and collection efficiencies, ultimately elevating system efficiency.

In 2023, Lu *et al.* incorporated a chlorophyll-derived biomaterial (H_2Chl) as a solid additive into the PM6:Y6 blend [89]. The BHJ film induced by H_2Chl demonstrated reduced intermolecular distances and tighter stacking. AFM results showed a slightly higher roughness (RMS = 1.00 nm) compared to the control film (RMS = 0.98 nm). H_2Chl introduction modulated self-assembly and crystalline stacking, enhancing crystallinity and charge transfer efficiency. Acting as a solid additive, H_2Chl elevated system efficiency from 15.97% to 17.30%. Its successful application offers insights for environmentally-friendly additives.

3.2. Volatile solid additives

Volatile solid additives exhibit volatility during post-processing steps like TA, leaving behind appropriate voids in the active layer film. This allows molecules in the photovoltaic layer to have room for movement and reorganization *in situ*, offering the potential for dynamic optimization of the film's morphology. It serves to regulate the active layer's morphology and establishes a foundation for long-term operational stability [90].

3.2.1. Phenyl derivatives

Non-fullerene acceptors are currently the most efficient materials for the active layer in OPVs. Molecules with electron-deficient end-groups, structurally similar to non-fullerene acceptors, uniquely regulate the acceptor in OPV. In 2019, Ma *et al.* introduced solid additives SA-4 and SA-7 into the PBDB-TF:IT-4F system [91], investigating changes in the active layer morphology. Both SA-4 and SA-7 blended films exhibited uniform surface morphologies and enhanced acceptor aggregation behavior (RMS = 2.75 nm, RMS = 2.75 nm), owing to high compatibility with IT-4F. After TA, the SA-7 blended film showed larger crystals and increased roughness (RMS = 3.02 nm, RMS = 9.27 nm), attributed to SA-7′s aggregation during heating and its lower volatility. This hindered complete departure from the active layer. SA-4 and SA-7 promote acceptor molecular packaging through intermolecular interactions with acceptor terminal groups during film formation, leading to more condensed IT-4F stacking after TA. Conversely, less volatile SA-7 either remains or aggregates on the surface, resulting in suboptimal device performance. Similarly, in 2021, Sun *et al.* employed IC-FI as a solid additive incorporated into the BTR-Cl:N3 system [92]. AFM results demonstrated that after IC-FI treatment, the film surface became smoother (RMS = 1.16 nm), enhancing phase separation within the active layer and forming a more interconnected

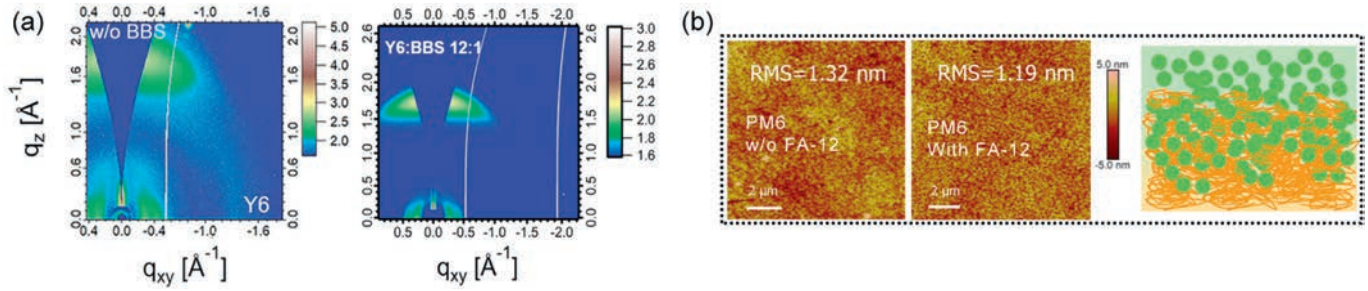

Fig. 7. (a) GIWAXS patterns of the neat Y6 film with or without BBS additive. Reproduced with permission [84]. Copyright 2022, John Wiley and Sons. (b) AFM images of the neat PM6 film with or without FA-12 additive, and scheme diagram of molecular stacking of the PM6:Y6 blend film with FA-12 additive. Reproduced with permission [88]. Copyright 2023, Springer Nature.

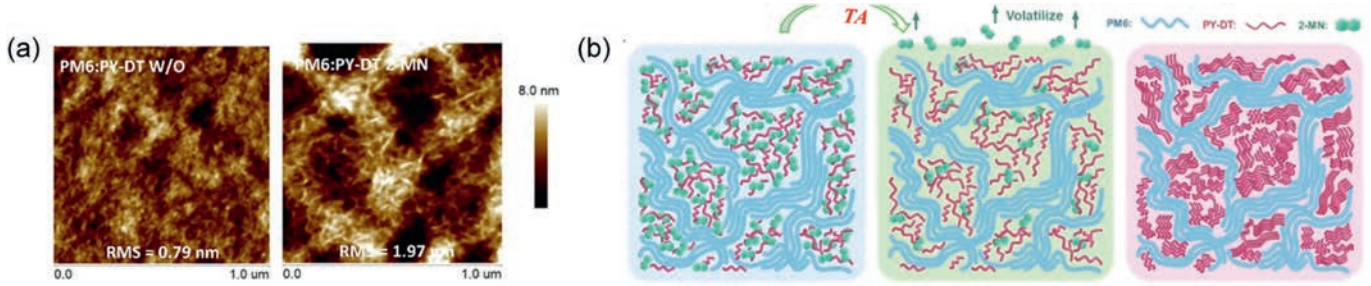

Fig. 8. (a) AFM height images of the PM6:PY-DT blend film with or without 2-MN additive. (b) Molecular arrangement diagram of the PM6:PY-DT blend film adding 2-MN before and after annealing. Reproduced with permission [93]. Copyright 2022, Elsevier.

network structure. GIWAXs results revealed compact stacking of molecules within the blend film with the addition of IC-FI as a solid additive. The study found that due to the structural similarity of IC-FI to the terminal of the N3 acceptor molecule, IC-FI could serve as a bridge to strengthen π-π interactions between adjacent N3 molecules and enhance compatibility between N3 and BTR-Cl. During annealing, the volatility of IC-FI effectively induced molecular aggregation, thereby regulating the microstructure of the active layer. This led to an efficiency enhancement from 13.36% to 14.43%. Recent researches indicate that IC-based volatile solid additives offer a simple and effective approach for modulating the morphology of organic active layers, achieving optimization through molecular stacking and nano-phase blending.

Due to the larger size of polymer molecules, their diffusion rates during active layer formation are slower compared to small molecules, often leading to unfavorable phase separation. In 2022, Sun *et al.* introduced 2-methoxynaphthalene (2-MN) into the PM6:PY-DT system for optimization [93]. AFM imaging (Fig. 8a) revealed that the 2-MN-treated blend exhibited a rougher surface (1.97 nm) compared to the control (RMS = 0.79 nm), indicating multi-scale phase separation domains. 2-MN effectively regulated PM6 and PY-DT aggregation at different film-forming stages. As demonstrated in Fig. 8b, during film formation, 2-MN induced strong PM6 aggregation improving molecular order to form an excellent fiber framework, and inhibiting PY-DT aggregation. With 2-MN gradually removal during thermal annealing, more space was created. This allowed PY-DT to aggregate, resulting in a more ordered stacking. This achieved a well-defined fibrous morphology, enhancing exciton dissociation and charge transport, and reducing trap-assisted recombination. 2-MN's use elevated efficiency from 14.47% to 17.32%.

In 2021, Cui *et al.* incorporated anthracene (An) as a solid additive into the PM6:Y6 system, elevating the system efficiency from 15.30% to 17.02% [94]. AFM analysis showed that both pristine PM6 and Y6 films exhibited uniformly smooth surfaces (RMS = 1.02 nm, and RMS = 2.12 nm, respectively) before and after thermal annealing. The introduction of anthracene, with its large crystals, led to notably rougher surfaces in the blend films PM6:An (RMS = 91.2 nm) and Y6:An (RMS = 32.3 nm). This effect stems from the high miscibility between anthracene and Y6, which restrains excessive aggregation of Y6 molecules during film formation. Furthermore, during thermal annealing, anthracene volatilizes, creating spaces where Y6 infiltrates the PM6 matrix, forming a dual-continuous interpenetrating network. Thus, this process significantly enhances charge separation and transport in the optimized system.

In 2023, Hou *et al.* introduced PDBB into the PM6:L8-BO system and observed that the addition of PDBB could make the morphology of the system smoother [44]. That same year, Kan *et al.* utilized the LbL process to introduce 1,3,5-tribromobenzene (TBB) into the acceptor section of the PM6:Y6 system [95], probing the additive's mechanism. The active layer's morphology presented a uniform, ordered molecular stacking in the TBB+TA-treated film. This suppressed bimolecular charge recombination and facilitated efficient charge transport. GIWAXs indicated shorter stacking distances in the blend film with the addition of TBB and TA. The pre-spin-coating process in D18-Cl:L8-BO system, face-to-face stacking in the donor layer was observed. Solvent permeation enabled mutual diffusion of donor and acceptor molecules, forming small mixed BHJ regions. Post-annealing, TBB completely volatilized, refining crystalline uniformity, enhancing phase purity, and displaying distinct vertical phase segregation. TBB addition raised system efficiency from 17.2% to 18.5%. In 2023, Hou *et al.* incorporated 1,3,5-trimethoxybenzene (TMB) into the PBDB-TF:eC9 system to study its impact on nanostructure and crystallinity [38]. GIWAXs results revealed that compared to DIO the TMB-treated blend film shows few diffraction peaks with broad distribution. As shown in Fig. 9a, TMB facilitated eC9 aggregation through electrostatic interactions during spin-coating's crystal growth stage, promoting phase separation with larger but loosely stacked π-π distances. Subsequently, TMB volatilized, leaving loosely packed eC9 aggregates. The mild thermally-induced aggregation allowed precise adjustment of acceptor's π-π stacking by varying annealing time, which results in enhanced exciton delocalization, efficient charge transfer, and in-

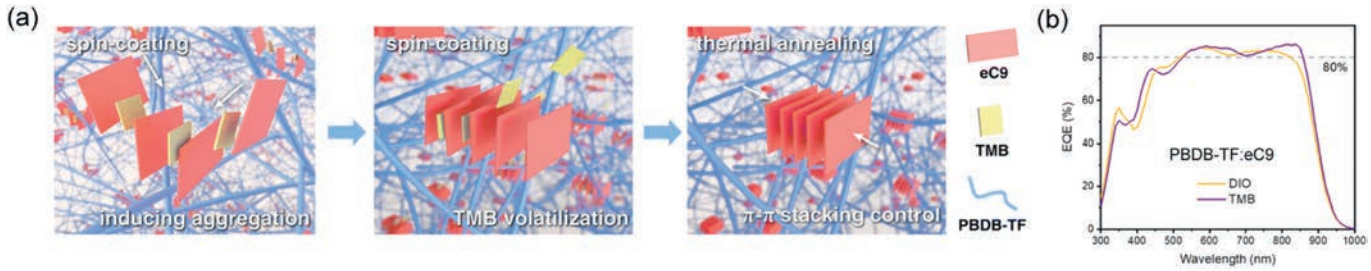

Fig. 9. (a) Molecular state scheme diagram of the PBDB-TF:eC9 blend film with TMB addition before and after TA. (b) EQE spectra of the device based on PBDB-TF:eC9 blend film with DIO or TMB additive. Reproduced with permission [38]. Copyright 2023, The Royal Society of Chemistry.

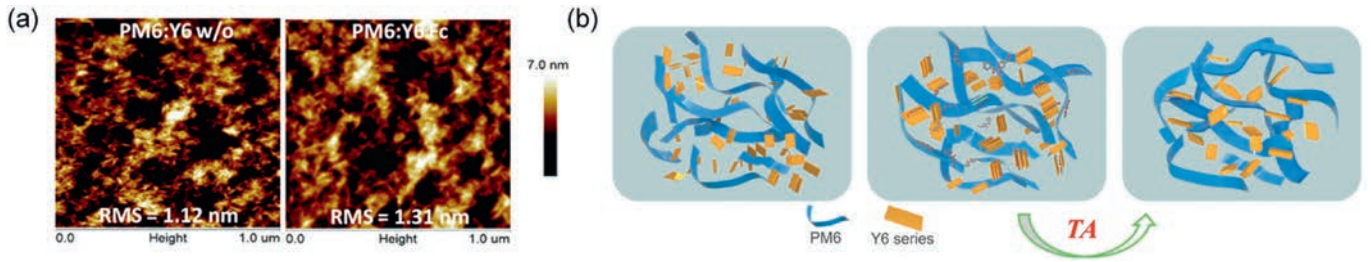

Fig. 10. (a) AFM height images of the PM6:Y6 blend film with or without Fc additive. Reproduced with permission [96]. Copyright 2023, The Royal Society of Chemistry. (b) Molecular state scheme diagram of the PM6:Y6 blend film with or without 2-HM additive before and after TA. Reproduced with permission [99]. Copyright 2023, John Wiley and Sons.

hibited non-radiative recombination loss. As shown in Fig. 9b, EQE reaches a high value beyond 86%, resulting in outstanding photovoltaic performance of 18.61%.

In summary, the simple structure addition based on the basic benzene ring makes such small molecules usually have a lower boiling point, which makes it easy to remove in the TA process, leaving a lot of space to provide the possibility of molecular rearrangement in the active layer, so it has excellent kinetic performance in OPV morphology optimization. However, these small molecules have different groups, so that they have different intermolecular interaction forces on the OPV system molecules before volatilization in the active layer, showing different results. This kind of small molecule solid additives has shown unique advantages in OPV morphology optimization.

3.2.2. Other types of volatile solid additives

In 2020, Sun *et al.* introduced ferrocene (Fc) as a solid additive into the PM6:Y6 system to enhance the active layer morphology [96]. Treated films displayed larger fiber width and higher phase separation (Fig. 10a, RMS = 1.31 nm). GIWAXs showed maintained face-face orientation with denser molecule stacking after Fc treatment, aiding vertical charge transport. During thermal annealing, Fc volatilized, expanding aggregation space for PM6 and Y6 to result in a more ordered structure. Ferrocene promoted improved phase separation and compact arrangement, boosting charge transport and suppressing recombination to achieve a notable efficiency enhancement. In 2021, Cui *et al.* introduced highly crystalline DDT as a solid additive to control the excessive self-assembly of non-fullerene acceptors during film formation [97], addressing limitations associated with CN solvents. AFM analysis revealed a uniformly smooth surface morphology after treatment with the CN and DTT mixture additive (RMS = 0.84 nm). This dual additive approach outperformed CN treatment alone in regulating phase separation. GIWAXs results indicated improved face-face stacking and π-π stacking distances. DTT, in conjunction with CN, effectively restricted Y6 molecule over-assembly during film formation. After TA and DTT removal, Y6 infiltrated the PM6 matrix, forming a nano-scale phase-separated dual-continuous interpenetrating network with fibrous features, and enhancing charge transport and extraction while suppressing recombination. Ultimately, DDT addition raised system efficiency from 15.74% to 16.97%. In 2022, Peng *et al.* further explored DDT's application in OPVs [98].

In 2023, Yuan *et al.* incorporated the novel solid small molecule, 2–hydroxy-4-methoxydibenzoylmethane (2-HM), into the PM6:Y6 system [99]. The films containing 2-HM exhibited slightly higher surface roughness than the original blend film (RMS = 0.91 nm). The addition of 2-HM induced a nano-scale network, leading to reduced phase separation dimensions. Subsequent annealing and volatilization of 2-HM brought about significant morphological changes, resulting in an enhanced interpenetrating D-A network structure and improved phase separation scale (RMS = 0.88 nm). The study highlighted that when processing PM6:Y6 films with pure chloroform solvent, rapid evaporation led to simultaneous formation of PM6 and Y6 crystalline molecules, causing extensive stacking and phase separation (Fig. 10b). The introduction of 2-HM had a more pronounced effect on the Y-series molecules. After annealing and the subsequent volatilization of 2-HM, PM6 and Y6 continued to assemble, forming a more densely ordered stacking structure. This proved advantageous for enhancing charge transport and extraction efficiency, while suppressing recombination.

4. Conclusions

Achieving the optimal morphology of the active layer is crucial for attaining effective performance in OPV devices, and the additive strategy has been proven as a viable and straightforward approach (through feasible ratio adjustments and BHJ process). This article elucidates the significance of the microstructure of the active layer in OPVs for exciton and charge carrier behavior, as well as its critical impact on device photovoltaic performance. Additives' roles are classified from both thermodynamic and kinetic perspectives, providing a detailed discourse on the regulatory effects and working mechanisms of different types of additives on the active layer morphology and their influence on device photovoltaic performance. From a thermodynamic standpoint, the role of liquid additives is expounded upon. This involves manipulating intra- and intermolecular interactions by exploiting the solubility disparities of active layer materials in solvents, thereby achieving optimiza-

tion of the blend film morphology. However, it is evident that traditional liquid additives pose potential risks to the long-term stability of the devices. In terms of kinetics, the function of solid additives is addressed. This encompasses regulation of the stacking and orientation of molecules after film formation through interactions between non-volatile solid additives and active layer molecules. Volatile solid additives, in combination with other post-processing techniques, facilitate the rearrangement of active layer molecules, leading to the optimization of thin film crystallinity and phase purity. While, currently developed solid additives exhibit system selectivity and lack high universality. In summary, the pivotal role of additives in the optimization of organic photovoltaic devices is underscored. Exploring and developing additives for organic photovoltaic active layers is of paramount importance for the industrialization of OPVs. Therefore, the quest for stable and efficient novel additives remains a critical task.

Declaration of competing interest

The authors declare that they have no known competing financial interests or personal relationships that could have appeared to influence the work reported in this paper.

Acknowledgments

This work is supported by the National Natural Science Foundation of China (Nos. 52303226, 21971049), Zhejiang Provincial Natural Science Foundation (Nos. LQ23E030002, LZ23B040001), and “Ten-thousand Talents Plan” of Zhejiang Province (No. 2019R52040).

References

[1] L. Duan, A. Uddin, Adv. Sci. 7 (2020) 1903259.
[2] Z. Jiang, K. Fukuda, W.C. Huang, et al., Adv. Funct. Mater. 29 (2019) 1808378.
[3] S. Xiong, K. Fukuda, S. Lee, et al., Adv. Sci. 9 (2022) 2105288.
[4] Y.Y. Zhou, M. Li, H. Lu, et al., Adv. Funct. Mater. 31 (2021) 2101742.
[5] R.J. Ma, C.Q. Yan, J.S. Yu, et al., ACS Energy Lett. 7 (2022) 2547–2556.
[6] K. Li, H. Zhen, L. Niu, et al., Adv. Mater. 26 (2014) 7271–7278.
[7] Y.B. Cheng, A. Pascoe, F. Huang, Y. Peng, Nature 539 (2016) 488–489.
[8] L. Sun, W. Zeng, C. Xie, et al., Adv. Mater. 32 (2020) 1907840.
[9] F. Li, F.R. Lin, A.K. Jen, Adv. Mater. (2023), doi:10.1002/adma.202307161.
[10] C.H. Zhang, S. Langner, A.V. Mumyatov, et al., J. Mater. Chem. A 5 (2017) 17570–17579.
[11] F. Gao, Joule 3 (2019) 908–909.
[12] W. Ma, X. He, T. Chen, et al., Chin. Chem. Lett. 35 (2024) 109099.
[13] Y.J. Cui, P.P. Zhu, X.X. Xia, et al., Chin. Chem. Lett. 34 (2023) 107902.
[14] M.R. Pu, C.C. Cao, H. Chen, et al., Chem. Eng. J. 437 (2022) 135198.
[15] X.Y. Du, X. Lu, J.W. Zhao, et al., Adv. Funct. Mater. 29 (2019) 1902078.
[16] Q.L. Song, H.B. Yang, Y. Gan, et al., J. Am. Chem. Soc. 132 (2010) 4554–4555.
[17] F. Pan, X.J. Li, S. Bai, et al., Chin. Chem. Lett. 32 (2021) 1257–1262.
[18] M. Günther, N. Kazerouni, D. Blätte, et al., Nat. Rev. Mater. 8 (2023) 456–471.
[19] L. Kaake, X.D. Dang, W.L. Leong, et al., Adv. Mater. 25 (2013) 1657 -1657.
[20] D. He, F.W. Zhao, C.R. Wang, Y.Z. Lin, Adv. Funct. Mater. 32 (2022) 2111855.
[21] J.Q. Mai, H.P. Lu, T.K. Lau, et al., J. Mater. Chem. A 5 (2017) 11739–11745.
[22] C.Y. Yang, S.Q. Zhang, J.Z. Ren, et al., Chin. Chem. Lett. 32 (2021) 2274–2278.
[23] D.H. Li, X. Zhang, D. Liu, T. Wang, J. Mater. Chem. A 8 (2020) 15607–15619.
[24] D. Li, C. Guo, X. Zhang, et al., Aggregate 3 (2022) e104.
[25] B. Siegmund, M.T. Sajjad, J. Widmer, et al., Adv. Mater. 29 (2017) 1604424.
[26] J. Chen, X. Chang, J. Guo, et al., Research 6 (2023) 0084.
[27] L. Ye, K. Weng, J. Xu, et al., Nat. Commun. 11 (2020) 6005.
[28] W. Zhang, Y. Wu, R. Ma, et al., Angew. Chem. Int. Ed. 62 (2023) e202309713.
[29] Y.A. Wei, J.W. Yu, L.Q. Qin, et al., Energy Environ. Sci. 14 (2021) 2314–2321.
[30] X.Y. Zhou, Y. Zhang, W.G. Kong, et al., J. Mater. Chem. A 6 (2018) 3012–3021.
[31] A.J. Bourque, S. Engmann, A. Fuster, et al., J. Mater. Chem. A 7 (2019) 16458–16471.
[32] J.M. Warman, M.P. de Haas, T.D. Anthopoulos, D.M. de Leeuw, Adv. Mater. 18 (2006) 2294–2298.
[33] K.X. Steirer, R.E. Richards, A.K. Sigdel, et al., J. Mater. Chem. A 3 (2015) 10949–10958.
[34] Z. Zhou, G. Liu, Small 13 (2017) 1603107.
[35] J. Zhou, X. Man, Y. Jiang, M. Doi, Adv. Mater. 29 (2017) 1703769.
[36] C. Ling, Y. Xia, X. Xiao, et al., Small Method 6 (2022) 2200161.
[37] R. Yu, G. Wu, Y. Cui, et al., Small 17 (2021) 2103497.
[38] Z.H. Chen, H.F. Yao, J.W. Wang, et al., Energy Environ. Sci. 16 (2023) 2637–2645.
[39] D.F. Zhang, Y.F. Li, M.J. Li, et al., Adv. Funct. Mater. 32 (2022) 2205338.
[40] J.H. Fu, H.Y. Chen, P.H. Huang, et al., Nano Energy 84 (2021) 105862.
[41] O. Alqahtani, J. Lv, T. Xu, et al., Small 18 (2022) 2202411.
[42] H. Liu, Y. Fu, Z. Chen, et al., Adv. Funct. Mater. 33 (2023) 2303307.
[43] Y.F. Zheng, J. Huang, G. Wang, et al., Mater. Today 21 (2018) 79–87.
[44] Y.F. Wang, Z.Z. Liang, X.F. Liang, et al., Adv. Energy Mater. 13 (2023) 2300524.
[45] Y.D. Zhang, Y. Cho, J. Lee, et al., J. Mater. Chem. A 8 (2020) 13049–13058.
[46] D. Hu, H. Tang, S. Karuthedath, et al., Adv. Funct. Mater. 33 (2023) 2211873.
[47] D.H. Lee, D.H. Kim, T. Kim, et al., Nano Energy 93 (2022) 106878.
[48] C. McDowell, M. Abdelsamie, M.F. Toney, G.C. Bazan, Adv. Mater. 30 (2018) 1707114.
[49] Y. Liu, B. Liu, C.Q. Ma, et al., Sci. China Chem. 65 (2022) 1457–1497.
[50] Y. Long, A.J. Ward, A. Ruseckas, I.D.W. Samuel, Synth. Met. 216 (2016) 23–30.
[51] X. Ma, Q. Jiang, W. Xu, et al., Chem. Eng. J. 442 (2022) 136368.
[52] S.J. Lou, N.J. Zhou, X.G. Guo, et al., J. Mater. Chem. A 6 (2018) 23805–23818.
[53] L.E. Garner, A. Bera, B.W. Larson, et al., ACS Energy Lett. 2 (2017) 1556–1563.
[54] K. Yamanaka, M. Saito, T. Koganezawa, et al., Adv. Energy Mater. 13 (2023) 2203443.
[55] J. Peet, C. Soci, R.C. Coffin, et al., Appl. Phys. Lett. 89 (2006) 252105.
[56] J.T. Rogers, K. Schmidt, M.F. Toney, et al., Adv. Mater. 23 (2011) 2284–2288.
[57] W.J. Wang, L. Song, D. Magerl, et al., Adv. Funct. Mater. 28 (2018) 1800209.
[58] J.K. Lee, W.L. Ma, C.J. Brabec, et al., J. Am. Chem. Soc. 130 (2008) 3619–3623.
[59] X. Wang, C. Feng, P. Liu, et al., Small 18 (2022) 2107106.
[60] H. Xu, Y. Yang, C. Zhong, et al., J. Mater. Chem. A 6 (2018) 6393–6401.
[61] S. Li, W. Liu, C.Z. Li, et al., Small 13 (2017) 1701120.
[62] C.V. Hoven, X.D. Dang, R.C. Coffin, et al., Adv. Mater. 22 (2010) E63–E66.
[63] D. He, F. Zhao, J. Xin, et al., Adv. Energy Mater. 8 (2018) 1802050.
[64] L. Ye, Y. Xiong, M.J. Zhang, et al., Nano Energy 77 (2020) 105310.
[65] L. Zhan, S. Li, X. Xia, et al., Adv. Mater. 33 (2021) 2007231.
[66] L. Ma, Y. Cui, J. Zhang, et al., Adv. Mater. 35 (2023) 2208926.
[67] T. Chen, X. Zheng, D. Wang, et al., Adv. Mater. 36 (2024) 2308061.
[68] M. Li, K. Xian, W. Zhao, et al., Chem. Eng. J. 476 (2023) 146723.
[69] B. Fan, W. Zhong, L. Ying, et al., Nat. Commun. 10 (2019) 4100.
[70] L. Chen, J. Yi, R. Ma, et al., Adv. Mater. 35 (2023) 2301231.
[71] X. Wang, L. Zhang, L. Hu, et al., Adv. Funct. Mater. 31 (2021) 2102291.
[72] K.E. Hung, Y.S. Lin, Y.J. Xue, et al., Adv. Energy Mater. 12 (2022) 2103702.
[73] N.J. Zhou, A. Facchetti, Mater. Today 21 (2018) 377–390.
[74] D. Wang, Z.F. Yang, F. Liu, et al., Chin. Chem. Lett. 33 (2022) 466–469.
[75] T. Kumari, S. Jung, Y. Cho, et al., Nano Energy 68 (2020) 104327.
[76] L. Liu, Y. Kan, K. Gao, et al., Adv. Mater. 32 (2020) 1907604.
[77] Y. Sun, L. Nian, Y. Kan, et al., Joule 6 (2022) 2835–2848.
[78] K. Sasitharan, R.C. Kilbride, E.L.K. Spooner, et al., Adv. Sci. 9 (2022) 2200366.
[79] S. Li, L. Zhan, Y. Li, et al., Small Method. 6 (2022) 2200828.
[80] Y.L. Yin, L.L. Zhan, M. Liu, et al., Nano Energy 90 (2021) 106538.
[81] X.Y. Kong, L.L. Zhan, S.X. Li, et al., Chem. Eng. J. 473 (2023) 145201.
[82] T. Yang, R.J. Ma, H. Cheng, et al., J. Mater. Chem. A 8 (2020) 17706–17712.
[83] M. Zhou, C. Liao, Y. Duan, et al., Adv. Mater. 35 (2023) 2208279.
[84] H. Lu, K. Chen, R.S. Bobba, et al., Adv. Mater. 34 (2022) 2205926.
[85] D. Wang, H.R. Liu, Y.H. Li, et al., Joule 5 (2021) 945–957.
[86] S. Zhang, L. Ye, H. Zhang, J. Hou, Mater. Today 19 (2016) 533–543.
[87] Y. Zhao, Z. Li, C. Deger, et al., Nat. Sustain. 6 (2023) 539–548.
[88] G. Ding, T. Chen, M. Wang, et al., Nano-Micro Lett. 15 (2023) 92.
[89] S. Duan, S.i. Sasaki, D. Han, et al., Adv. Funct. Mater. 33 (2023) 2302820.
[90] J. Wang, Y. Wang, P. Bi, et al., Adv. Mater. 35 (2023) 2301583.
[91] R. Yu, H. Yao, Z. Chen, et al., Adv. Mater. 31 (2019) 1900477.
[92] S.S. Chen, J.F. Ye, Q.G. Yang, et al., J. Mater. Chem. A 9 (2021) 2857–2863.
[93] J.L. Song, Y. Li, Y.H. Cai, et al., Matter 5 (2022) 4047–4059.
[94] H.Y. Fan, H. Yang, Y. Wu, et al., Adv. Funct. Mater. 31 (2021) 2103944.
[95] C. Zhu, S. Chung, J. Zhao, et al., Adv. Sci. 10 (2023) 2303150.
[96] L.L. Ye, Y.H. Cai, C. Li, et al., Energy Environ. Sci. 13 (2020) 5117–5125.
[97] S. Bao, H. Yang, H. Fan, et al., Adv. Mater. 33 (2021) 2105301.
[98] K. Chong, X. Xu, H. Meng, et al., Adv. Mater. 34 (2022) 2109516.
[99] X. Yang, B. Li, X. Zhang, et al., Adv. Mater. 35 (2023) 2301604.